

Publication status: This preprint has been published elsewhere.
DOI of the published preprint: <https://doi.org/10.36561/ING.30.16>

Simulation of fully developed laminar free convection flow between vertical parallel flat plates

Hector Espinoza-Roman

<https://doi.org/10.1590/SciELOPreprints.13568>

Submitted on: 2025-09-29

Posted on: 2026-01-27 (version 2)
(YYYY-MM-DD)

Version justification: In this version, the problem statement was added, the graphs were revised, and comparison tables were included.

Research article / *Article de recherche*

Simulation of fully developed laminar free convection flow between vertical parallel flat plates

Hector G. Espinoza-Roman , *, ^a^a Fundacion Universitaria Antonio de Arevalo UNITECNAR, 49A St. 31-45, Cartagena de Indias, Colombia. <https://orcid.org/0000-0002-2861-2442>*E-mail:* hector.espinoza@unitecnar.edu.co (H. Espinoza)

Abstract. This study presents a numerical investigation of laminar free convection flow between vertical parallel flat plates subjected to asymmetric uniform wall temperatures. The left and right walls are maintained at constant but different temperatures, with the right wall being hotter. A fluid at a uniform temperature, less than or equal to the cooler left wall temperature, enters the channel. The governing equations are solved using the finite volume method in OpenFOAM v13. A grid convergence study is conducted using systematically refined meshes to ensure the spatial independence of the results. The numerical solutions demonstrate excellent agreement with classical analytical profiles for fully developed flow. The linear analytical temperature profile is accurately captured even on coarser grids. In contrast, the cubic velocity profile requires more grid resolution to be precisely reproduced. The results validate the numerical methodology and provide insight into the mesh requirements for accurately simulating such natural convection flows.

Keywords. heat transfer, passive ventilation, solar chimney, CFD.

Funding. The first author is supported by Fundacion Universitaria Antonio de Arevalo project SSC through grant #2025-007.

Electronic supplementary material. Supplementary material for this article is supplied as a separate archive available from the journal's website under article's URL or from the author.

This article is a draft (not yet accepted)

1. Introduction

The motivation of this article is to serve as a starting point for the simulation of solar chimneys. Free convection is the driving force that generates flow in a solar chimney. The steady-state, fully developed laminar free convection between parallel flat plates is one of the most basic cases of free convection. Additionally, it has an analytical solution, which allows for a direct comparison and validation of simulation results in terms of velocity, temperature, pressure, and flow rate.

Solar chimneys, as a passive and sustainable ventilation and energy generation technology, have been the subject of extensive recent research. Contemporary studies have focused on optimizing their complex geometries, including roof-mounted configurations [1–3], high-rise designs for uniform flow [4, 5], and folded or curved façades [6, 7]. The performance of these systems under various climatic conditions and integration with other building components, such

*Corresponding author

as earth-to-air heat exchangers [8] or within specific building types like aged-care centers [9] and urban tunnels [10], has been rigorously investigated. Furthermore, comprehensive reviews by [11] and [12] underscore the maturity of the field while highlighting the persistent reliance on Computational Fluid Dynamics (CFD) as a primary investigative tool.

The accuracy of any CFD simulation for such applications, however, is fundamentally dependent on the proper resolution of the buoyancy-driven flow physics at its core. Before tackling the geometrical and turbulent complexities of real-world solar chimneys, it is imperative to ensure that the numerical methodology can precisely reproduce the underlying convective phenomena. The canonical case of laminar free convection between vertical, asymmetrically heated parallel plates serves as a critical benchmark for this purpose [13–18]. This flow configuration is not only representative of the core physics in a solar chimney’s flow channel but also possesses a well-established analytical solution [13, 14] providing an unambiguous standard for code verification.

While Direct Numerical Simulation (DNS) studies of turbulent flows in similar configurations exist [19], and several authors have employed CFD for performance analysis [20, 21], a clear gap remains in the literature regarding the meticulous verification of the numerical schemes and mesh requirements specifically for the laminar case using open-source CFD software OpenFOAM. Many studies proceed directly to complex applications without first demonstrating that their solver can accurately capture the basic velocity and temperature profiles that form the building blocks of the flow. This step is crucial for gaining confidence in simulation results, as errors introduced at this fundamental level can propagate and be amplified in more complex cases.

Therefore, this study aims to bridge this gap by presenting a detailed numerical investigation of the thermally developing, laminar free convection between vertical parallel plates with asymmetric uniform wall temperatures. Using the open-source CFD toolbox OpenFOAM, we systematically perform a grid convergence study to establish the mesh independence of the results. The primary objective is to validate the numerical methodology by demonstrating its ability to asymptotically approach the classical analytical solutions for both the temperature and velocity profiles in the fully developed regime. By doing so, this work provides a verified foundation upon which more complex simulations of solar chimneys and other natural convection applications can be reliably built.

2. Problem statement

This section details the equations that govern the laminar free convection between vertical parallel plates as well as the boundary conditions and adimensionalization of equations and variables.

2.1. Governing Equations

The flow is assumed to be two-dimensional, steady, incompressible and laminar. The Boussinesq approximation is adopted to model the buoyancy force, whereby density variations are considered only in the body force term of the momentum equation. Under these assumptions, the governing equations for conservation of mass, momentum, and energy are given by:

$$\nabla \cdot \mathbf{u} = 0, \quad (1)$$

$$\mathbf{u} \cdot \nabla \mathbf{u} + \frac{1}{\rho} \nabla p - \nu \Delta \mathbf{u} = \beta(T - T_0) \mathbf{g}, \quad (2)$$

$$\mathbf{u} \cdot \nabla T - \alpha \Delta T = 0, \quad (3)$$

where \mathbf{u} is the velocity vector, p is the pressure, T is the temperature, \mathbf{g} is the gravitational acceleration vector, ρ is the reference density, ν is the kinematic viscosity, $\alpha = k/(\rho c)$ is the thermal diffusivity, β is the thermal expansion coefficient and T_0 is the reference temperature.

2.2. Dimensionless Governing Equations

The dimensionless governing equations [13, 14], taking into account that $U = 0$, $V(X)$ and $\theta(X)$ are:

$$\frac{dP}{dX} = 0, \quad (4)$$

$$\frac{dP}{dY} - \frac{d^2V}{dX^2} = \theta, \quad (5)$$

$$-\frac{d^2\theta}{dX^2} = 0, \quad (6)$$

where,

$$X = \frac{x}{b}, \quad Y = \frac{y}{lGr}, \quad (7)$$

$$U = \frac{bu}{\nu}, \quad V = \frac{b^2v}{l\nu Gr}, \quad (8)$$

$$P = \frac{(p - p_0)b^4}{\rho l^2 \nu^2 Gr^2}, \quad \theta = \frac{T - T_0}{T_1 - T_0}, \quad (9)$$

$$Pr = \frac{\mu c}{k}, \quad Gr = \frac{g\beta(T_1 - T_0)b^4}{l\nu^2}. \quad (10)$$

The temperature difference ratio r_T is defined as:

$$r_T = \frac{T_2 - T_0}{T_1 - T_0}, \quad (11)$$

whereas the dimensionless flow rate is:

$$M = \frac{u_0 b^2}{l\nu Gr}. \quad (12)$$

2.3. Dimensionless Exact Solution

The exact solution [13, 14] for dimensionless velocity, pressure and temperature is:

$$U = 0, \quad (13)$$

$$V = (r_T - 1)\frac{X^3}{6} - r_T\frac{X^2}{2} + (2r_T + 1)\frac{X}{6}, \quad (14)$$

$$P = 0, \quad (15)$$

$$\theta = (1 - r_T)X + r_T. \quad (16)$$

The volumetric flow rate is:

$$M = \frac{r_T + 1}{24}. \quad (17)$$

The dimensionless average velocity is:

$$U_0 = M. \quad (18)$$

The dimensionless coordinate of the maximum velocity is:

$$X_{\max} = \frac{2r_T + 1}{3r_T + 1}, \quad (19)$$

where $A = \sqrt{3(r_T^2 + r_T + 1)}$.

The dimensionless maximum velocity is:

$$U_{\max} = \frac{X_{\max}}{18} [3(2r_T + 1) - (6r_T + A)X_{\max}]. \quad (20)$$

2.4. Domain and Boundary Conditions

The domain is a two-dimensional vertical channel of height L and gap width b , as illustrated in Figure 1.

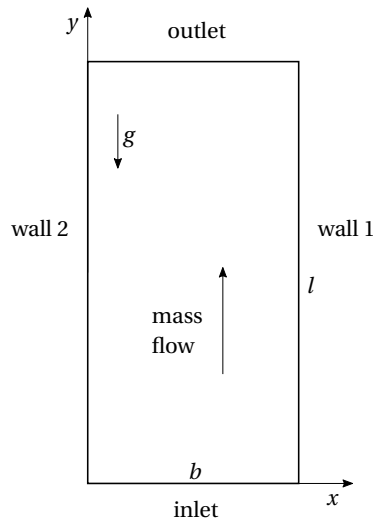


Figure 1. Schematic of the computational domain and boundary conditions.

The following boundary conditions are applied:

- **Right Wall (hot):** No-slip velocity condition $\mathbf{u} = \mathbf{0}$ and uniform wall temperature $T = T_1$.
- **Left Wall (cold):** No-slip velocity condition $\mathbf{u} = \mathbf{0}$ and uniform wall temperature $T = T_2$.
- **Inlet (bottom):** uniform pressure $p = 0$ and linear temperature variation $T(x = 0) = T_2$ and $T(x = b) = T_1$.
- **Outlet (top):** uniform pressure $p = 0$ with zero-gradient for velocity and temperature.

The average temperature is defined as:

$$\bar{T} = \frac{T_1 + T_2}{2}, \quad (21)$$

and the average temperature difference is:

$$\overline{\Delta T} = \bar{T} - T_0. \quad (22)$$

2.5. Fluid properties, domain size and boundary values

The values used for the simulation are for air at atmospheric pressure and temperature of 30 C. The values are summarized in Table 1.

Table 1. Values of magnitudes and derived magnitudes.

Magnitude	Value	Derived Magnitude	Value
g	9.8 m/s ²	\overline{T}	40 °C
T_0	30 °C	ν	1.608E-5 m ² /s
T_1	42.5 °C	k	0.02588 W/(m K)
T_2	37.5 °C	α	2.208E-5 m ² /s
b	0.005 m	Gr	0.6512
l	1.5 m	r_T	0.6
ρ	1.164 kg/m ³	$\overline{\Delta T}$	10 °C
β	3.299E-3 1/K	-	-
c	1007 J/(kg K)	-	-
μ	1.872E-5 Pa s	-	-
Pr	0.7282	-	-

3. Numerical simulation procedure

The open-source Computational Fluid Dynamics (CFD) toolbox OpenFOAM (version v13) was used to solve the governing equations (1)–(3). The steady-state solver `fluid`, which implements the SIMPLE (Semi-Implicit Method for Pressure-Linked Equations) algorithm for pressure-velocity coupling, was employed.

The spatial discretization schemes were first-order accurate. The Gauss linear scheme was used for the gradient terms, the bounded Gauss upwind scheme was used for the divergence terms and the Gauss linear corrected scheme was used for the Laplacian terms. An under-relaxation factor of 0.8 was applied to ensure numerical stability during the iterative solution process. Simulations were considered converged when the normalized residuals for all variables fell below 10^{-8} . More details of the exact set up can be seen in the OpenFOAM case file.

3.1. Mesh Independence Study

A systematic grid convergence study was conducted to ensure that the numerical results were independent of the mesh resolution. Three sequentially refined structured meshes were generated, characterized by an increasing number of cells in the transverse direction to better resolve the fluid field. The details of these meshes are provided in Table 2.

Table 2. Details of the meshes used for the grid convergence study.

Mesh	Number of Cells ($N_x \times N_y$)	Total Cells
Mesh04	4 × 100	400
Mesh08	8 × 100	800
Mesh16	16 × 100	1,600

4. Results and discussion

This section presents and discusses the numerical results obtained from the simulations of fully developed laminar free convection flow in a vertical channel. The primary objective is to validate the computational methodology by comparing the predicted temperature and velocity profiles

against the analytical solution. The influence of mesh resolution on the accuracy of these profiles is examined in detail.

The fully developed profiles were measured at 80% of channel height H in order to be sufficiently downstream of the flow and to have a reasonable separation from the outlet boundary.

4.1. Temperature Profile

Figure 2 shows the dimensionless temperature profile, θ , across the channel width for the three meshes alongside the analytical solution. As anticipated by the linear form of the analytical solution for the temperature field in the fully developed region, the numerical method reproduces it with exceptional accuracy across all mesh resolutions, including the coarsest mesh. The profiles are visually indistinguishable from the analytical line.

The correct imposition of the Dirichlet boundary conditions is confirmed by the data points at the walls; the dimensionless temperature at the left wall ($X = 0$) is $\theta = 0.0$ and at the right wall ($X = 1$) is $\theta = 1.0$, exactly as specified. This perfect agreement is expected for a linear profile, as it can be exactly captured by the linear shape functions of the finite volume method, even with a minimal number of cells. This result serves as a primary check, verifying that the thermal boundary conditions and the energy equation discretization have been imposed correctly.

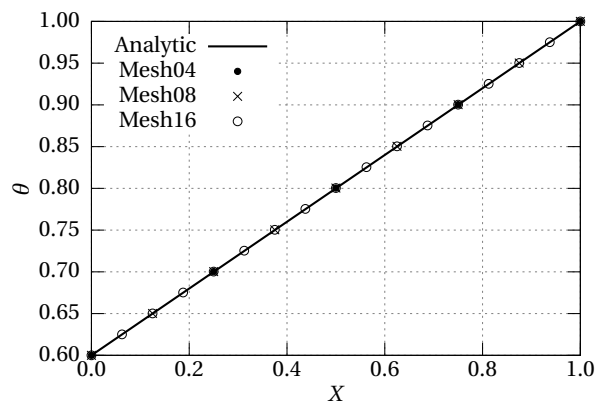


Figure 2. Temperature profile.

4.2. Velocity Profile

The validation of the velocity field presents a more stringent test for the numerical method. Figure 3 displays the dimensionless vertical velocity profile, V , for the three meshes compared to the analytical solution. Velocity was extracted from the mesh by sampling using an interpolation scheme `cellPoint` of type `lineFace`.

The no-slip boundary condition is correctly satisfied on both walls ($X = 0, V = 0$ and $X = 1, V = 0$) for all meshes. The location and value of the maximum velocity near the channel centerline ($X \approx 0.5$) are also captured remarkably well, even on the coarsest mesh. Additionally, it is impressive how, even the coarsest mesh, captures the velocity profile very well.

In order to see the velocity profile by cell values, velocity is plotted in Figure 4. Velocity was extracted from the mesh by sampling using an interpolation scheme `cell` of type `lineCell`. This just takes the cell values (velocity and coordinate) without interpolation. In this figure, the

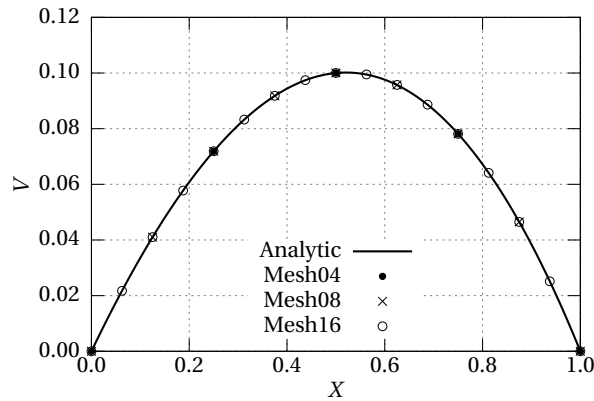


Figure 3. Vertical velocity profile.

differences between meshes can be seen more clearly: coarsest mesh produces the less accurate result and the finest mesh produces the most accurate result as expected. Anyway, it is still impressive how even Mesh04 approximates the exact solution.

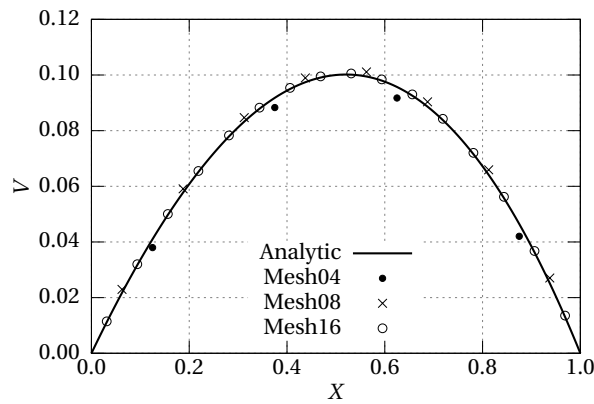


Figure 4. Vertical velocity profile (cell).

4.3. Pressure Profile

Figure 5 displays the dimensionless pressure profile, P , for the three meshes compared to the analytical solution. Pressure is correctly captured by all the meshes.

4.4. Quantitative Error Analysis

To move beyond a visual comparison, a quantitative analysis of the discretization error was performed. The relative error in the maximum velocity ($\epsilon_{V_{max}}$) and the relative error in the position of the maximum velocity ($\epsilon_{X_{max}}$) were calculated for each mesh relative to the analytical solution. The results are summarized in Table 3. It can be seen that the error in the maximum

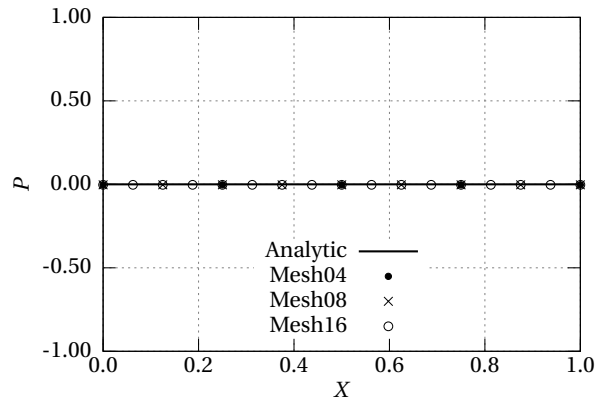


Figure 5. Pressure profile.

velocity is already very small in the coarse mesh and there is very little improvement in the finer meshes. The error in the position of the maximum velocity as well stays constant, but this is because Mesh04 to Mesh16 do not capture the maximum velocity position well. We have to point out that, for this case, the exact velocity profile is not symmetric and the maximum velocity is reached at $X = 0.5207$. However, the meshes we are using do not capture that point closely. To overcome that, a mesh with 15 divisions is added to the table and it shows better agreement with the maximum velocity and position.

Table 3. Quantitative error analysis for the maximum vertical velocity.

Mesh	X_{\max}	$\epsilon_{X_{\max}}$ (%)	V_{\max}	$\epsilon_{V_{\max}}$ (%)
Mesh04	0.5000	-3.98	0.1000249	0.15
Mesh08	0.5000	-3.98	0.1000257	0.15
Mesh16	0.5000	-3.98	0.1000259	0.15
Mesh15	0.5333	2.42	0.1001343	0.04
Analytical	0.5207	–	0.1001730	–

Now, in order to compare quantitatively the cell velocity, Table 4 shows the error in the maximum cell velocity value and position. It can be seen the convergence in the the maximum velocity position as well as the convergence on the maximum velocity value.

Table 4. Quantitative error analysis for the maximum vertical velocity (cell).

Mesh	X_{\max}	$\epsilon_{X_{\max}}$ (%)	V_{\max}	$\epsilon_{V_{\max}}$ (%)
Mesh04	0.62500	20.0	0.0917403	-8.42
Mesh08	0.56250	8.02	0.1010997	0.92
Mesh16	0.53125	2.02	0.1005507	0.38
Analytical	0.52072	–	0.1001730	–

Let us now compare the dimensionless volumetric flow rate M . Flow rate is a key magnitude to have into account when analyzing solar chimneys for ventilation. Table 5 shows the volumetric flow rate and its error for various meshes. It can be seen the monotonous convergence of M when refining the mesh.

Table 5. Quantitative error analysis for volumetric flow rate.

Mesh	M	ϵ_M (%)
Mesh04	0.0750164	12.5
Mesh08	0.0687656	3.15
Mesh16	0.0672029	0.80
Mesh32	0.0668121	0.22
Mesh64	0.0667140	0.07
Analytical	0.0666667	–

Let us focus now on mass flow rate. Table 6 shows the mass flow rate for various meshes. The dimensional mass flow rate (\dot{m}) was computed taking the depth of the channel equal to its width. The dimensionless numerical mass flow rate was computed by first converting the mass flow rate to volumetric flow rate using density at \bar{T} and then adimensionalizing this value. The exact dimensionless mass flow rate was taken equal to the dimensionless volumetric flow rate.

Table 6. Quantitative error analysis for mass flow.

Mesh	\dot{m} (kg/s)	\dot{M}	$\epsilon_{\dot{M}}$ (%)
Mesh04	1.3260E-6	0.0750011	12.5
Mesh08	1.2156E-6	0.0687545	3.13
Mesh16	1.1880E-6	0.0671930	0.79
Mesh32	1.1811E-6	0.0668025	0.20
Mesh64	1.1793E-6	0.0667045	0.06
Analytical	1.1794E-6	0.0666667	–

Finally, let us analyze the y^+ . It is denoted yPlus in OpenFOAM notation. Table 7 shows y^+ on the left and right wall for various meshes. It can be seen that even for the coarsest mesh it has a quite good value nearly 1. For the finer meshes, y^+ is sufficiently good.

Table 7. Values of y^+ for various meshes.

Mesh	$y^+(X=0)$	$y^+(X=1)$
Mesh04	1.04	1.12
Mesh08	0.52	0.56
Mesh16	0.26	0.28

5. Conclusion

This study has successfully conducted a detailed numerical verification of laminar free convection in a vertical channel with asymmetric wall temperatures, serving as a foundational benchmark for simulating more complex systems like solar chimneys. The key findings and implications of this work are summarized as follows:

1. Successful Methodology Validation: The implemented model in OpenFOAM v13 has demonstrated a robust capability for simulating buoyancy-driven flows. The numerical solutions showed excellent agreement with the analytical profiles for the fully developed region, thereby validating the chosen computational approach and the implementation of the physical models.

2. **Critical Role of Mesh Resolution:** A systematic grid convergence study revealed a distinct sensitivity to mesh density based on the flow variable of interest. The linear temperature profile, characteristic of the fully developed thermal field, was accurately reproduced even on relatively coarse meshes. In contrast, the cubic velocity profile, required progressively finer meshes to be captured with high fidelity. However, it is impressive how the model captures the velocity profile even for the coarsest mesh. This underscores the importance of a mesh-independent study and indicates that the velocity field is the more critical metric for determining sufficient spatial resolution in this type of simulation.

3. **Practical Implications for Solar Chimney Simulation:** The findings provide a crucial practical guideline for CFD modeling of solar chimneys and similar passive ventilation systems. While simplified models might adequately predict temperature distributions, accurate prediction of air-flow rates, which is directly tied to the velocity profile, requires a certain grid resolution. This insight is essential for optimizing computational resources without sacrificing the accuracy of key performance metrics, such as ventilation flow rate.

4. **Foundation for Future Work:** This rigorously verified setup forms a reliable foundation for subsequent research. The validated methodology can be confidently extended to investigate more complex and realistic scenarios, including turbulent flow regimes, geometrically complex channels relevant to advanced solar chimney designs and transient solar loading conditions.

In conclusion, this work reaffirms the necessity of fundamental verification as a critical first step in computational fluid dynamics. By establishing a benchmark for accuracy in a canonical case, it enhances the reliability of future numerical studies aimed at optimizing and designing efficient natural convection systems for sustainable building engineering.

Conflict of interest

The authors declare no competing financial interest.

Dedication

The manuscript was written through contributions of all authors. All authors have given approval to the final version of the manuscript.

Acknowledgments

The author is supported by Fundacion Universitaria Antonio de Arevalo UNITECNAR through grant #2025-007.

Research data availability

Data is available on request to the corresponding author. The research data is available on demand.

References

- [1] C. Wang, Y. Wu, C. Hua, X. Zhao, J. Zang, N. Gao, "Numerical investigation on the influence of geometric parameters on turbulent flow and thermal performance in the roof solar chimney", *Building and Environment* **267** (2025), p. 112210.
- [2] A. Vazquez-Ruiz, J. M. A. Navarro, J. F. Hinojosa, J. P. Xamán, "Effect of the solar roof chimney position on heat transfer in a room", *International Journal of Mechanical Sciences* **209** (2021), p. 106700.

- [3] A. Vazquez-Ruiz, J. M. A. Navarro, J. F. Hinojosa, J. P. Xamán, “Computational Fluid Dynamics and Experimental Analysis of the Heat Transfer in a Room With a Roof Solar Chimney”, *Journal of Thermal Science and Engineering Applications* **14** (2022), no. 4, p. 041001.
- [4] J. Gong, L. W. Chew, P. S. Lee, “Shape optimization of high-rise solar chimneys to improve the uniformity of flowrate distribution”, *Building and Environment* **243** (2023), p. 110650.
- [5] J. Gong, L. W. Chew, P. S. Lee, “Theoretical model for high-rise solar chimneys and optimum shape for uniform flowrate distribution”, *Energy* **298** (2024), p. 131358.
- [6] J. Ahmadi, M. Mahdavejad, S. Asadi, “Folded double-skin façade (DSF): in-depth evaluation of fold influence on the thermal and flow performance in naturally ventilated channels”, *International Journal of Sustainable Energy* **41** (2022), no. 4, p. 382-411.
- [7] Y. Huang, Y. Tao, L. Shi, Q. Liu, Y. Wang, J. Tu, Q. Peng, C. Cao, “Thermal and ventilation performance of a curved double-skin facade model”, *Energy and Buildings* **268** (2022), p. 112202.
- [8] F. Pouranian, H. Akbari, S. M. Hosseinalipour, “Performance assessment of solar chimney coupled with earth-to-air heat exchanger: A passive alternative for an indoor swimming pool ventilation in hot-arid climate”, *Applied Energy* **299** (2021), p. 117201.
- [9] Q. Wang, G. Zhang, Q. Wu, L. Shi, “Ventilating aged-care center based on solar chimney: Design and theoretical analysis”, *Energy and Buildings* **266** (2022), p. 112145.
- [10] Y. Huang, X. Liu, L. Shi, B. Dong, H. Zhong, “Enhancing solar chimney performance in urban tunnels: Investigating the impact factors through experimental and theoretical model analysis”, *Energy* **282** (2023), p. 128329.
- [11] B. Zamora, “A review on solar chimneys: from natural convection fundamentals to thermohydraulic best-performance proposals”, *Processes* **11** (2023), no. 2, p. 386.
- [12] S. P. Melgaard, I. T. Nikolaiisson, C. Zhang, H. Johra, O. K. Larsen, “Double-skin façade simulation with computational fluid dynamics: A review of simulation trends, validation methods and research gaps”, *Building Simulation* **16** (2023), no. 12, p. 2307-2331.
- [13] W. Aung, L. Fletcher, V. Sernas, “Developing laminar free convection between vertical flat plates with asymmetric heating”, *International Journal of Heat and Mass Transfer* **15** (1972), no. 11, p. 2293-2308.
- [14] W. Aung, “Fully developed laminar free convection between vertical plates heated asymmetrically”, *International Journal of Heat and Mass Transfer* **15** (1972), no. 8, p. 1577-1580.
- [15] W. Aung, G. Worku, “Developing flow and flow reversal in a vertical channel with asymmetric wall temperatures”, *ASME Journal of Heat Transfer* **108** (1986), no. 2, p. 299-304.
- [16] N. Anand, S. Kim, L. Fletcher, “The effect of plate spacing on free convection between heated parallel plates”, *ASME Journal of Heat Transfer* **114** (1992), no. 2, p. 515-518.
- [17] “Laminar natural convection between vertical isothermal heated plates with different temperatures”.
- [18] S. Froushani, D. Naylor, J. L. Wright, “Heat transfer correlations for laminar free convection in vertical channels with asymmetrically heated isothermal walls”, *Heat Transfer Engineering* **41** (2020), p. 5.
- [19] J. Pallares, A. Fabregat, C. Lei, “Direct numerical simulation of the fully developed turbulent free convection flow in an asymmetrically heated vertical channel”, *International Journal of Thermal Sciences* **191** (2023), p. 108352.
- [20] A. H. Radwan, M. M. S. Ahmed, “Improving thermal performance and air flow inside the solar chimney by CFD simulation”, *MSA Engineering Journal* **2** (2023), no. 2, p. 1245-1277.
- [21] S. Rodriguez Miranda, G. O. Gamboa, M. A. Zamora-Antuñano, N. Farrera-Vázquez, R. García-García, “CFD Evaluation of Thermal Conditioning in a House of Social Interest with a Solar Chimney Arrangement in Guanajuato, Mexico”, *Processes* **11** (2023), no. 4, p. 1286.
- [22]
- [23] C.-S. Ahn, B.-H. Bang, C. Park, D.-Y. Kim, A. L. Yarin, S. S. Yoon, “Experimental, analytical, and computational study of natural convection in asymmetrically-heated vertical shafts”, *International Journal of Thermal Sciences* **170** (2021), p. 107131.
- [24] K. Tesch, M. Ryms, W. M. Lewandowski, “Verification of the method of reconstructing convective velocity fields on the basis of temperature fields in vertical, differential and equally heated, open and closed channels”, *International Journal of Heat and Mass Transfer* **183** (2022), p. 122238.
- [25] M. Ryms, K. Tesch, W. M. Lewandowski, “Optimization of the distance between the vertical plates in the convective air heat exchanger”, *International Journal of Thermal Sciences* **185** (2023), p. 108064.
- [26] A. Zoubir, R. El Otmami, R. Bouferra, L. Essaleh, “Effects of thermal stratification on natural convection in a symmetrically heated channel: Comparison of characteristic quantities between air and water”, *Case Studies in Thermal Engineering* **45** (2023), p. 102950.
- [27] M. Dhahri, S. Nekoonam, A. Hana, M. El Haj Assad, M. Arici, M. Sharifpur, H. Sammouda, “Thermal performance modeling of modified absorber wall of solar chimney-shaped channels system for building ventilation”, *Journal of Thermal Analysis and Calorimetry* **145** (2021), p. 1137-1149.
- [28] Y. Tao, H. Zhang, L. Zhang, G. Zhang, J. Tu, L. Shi, “Ventilation performance of a naturally ventilated double-skin façade in buildings”, *Renewable Energy* **167** (2021), p. 184-198.

- [29] J. Ahmadi, M. Mahdavinjad, O. K. Larsen, C. Zhang, A. Zarkesh, S. Asadi, "Evaluating the different boundary conditions to simulate airflow and heat transfer in Double-Skin Facade", *Building Simulation* **15** (2022), p. 799-815.
- [30] A. Bouchair, "The effect of the altitude on the performance of a solar chimney", *Energy* **249** (2022), p. 123704.
- [31] J. Gong, K. X. Cheng, H. Liu, L. W. Chew, P. S. Lee, "A novel staggered split absorber design for enhanced solar chimney performance", *Building and Environment* **224** (2022), p. 109569.
- [32] A. Jankovic, M. S. Siddiqui, F. Goia, "Laboratory testbed and methods for flexible characterization of thermal and fluid dynamic behaviour of double skin facades", *Building and Environment* **210** (2022), p. 108700.
- [33] Q. Wang, G. Zhang, Q. Wu, L. Shi, "Solar chimney performance in buildings under three heating modes: An empirical analysis", *Sustainable Energy Technologies and Assessments* **52** (2022), p. 102222.
- [34] B. Zamora, "Morphological comparative assessment of a rooftop solar chimney through numerical modeling", *International Journal of Mechanical Sciences* **227** (2022), p. 107441.
- [35] S. Pastori, M.-S. Salehi, S. Radl, E. S. Mazzucchelli, "A Fast-Calibrated Computational Fluid Dynamic Model for Timber-Concrete Composite Ventilated Façades", *Buildings* **14** (2024), no. 11, p. 3567.
- [36] E. Iavorschi, L. D. Milici, P. Atănăsoae, C. Ungureanu, "An Experimental and Numerical Investigation of a Passive Façade and Proposals for Improving Its Energy Performance", *Energies* **18** (2025), no. 2, p. 359.
- [37] T. B. Korkut, A. Rachid, "Numerical investigation of interventions to mitigate heat stress: A case study in Dubai", *Energies* **17** (2024), no. 10, p. 2242.
- [38] A. Jankovic, F. Goia, "Impact of double skin facade constructional features on heat transfer and fluid dynamic behaviour", *Building and Environment* **196** (2021), p. 107796.
- [39] Y.-I. Song, K. Sheykhi Darani, A. I. Khdaif, G. Abu-Rumman, R. Kalbasi, "A review on conventional passive cooling methods applicable to arid and warm climates considering economic cost and efficiency analysis in resource-based cities", *Energy Reports* **7** (2021), p. 2784-2820.
- [40] N. El Zein, P. Désévaux, S. Bégot, Y. Ait Oumeziane, V. Lepiller, "Review of the experimental studies on trombe walls hygrothermal performance: a special focus on the PIV application in such a system", *Journal of Building Engineering* **98** (2024), p. 111321.
- [41] R. Zhang, X. Xu, K. Liu, L. Kong, W. Wang, T. Wortmann, "Airflow modelling for building design: A designers' review", *Renewable and Sustainable Energy Reviews* **197** (2024), p. 114380.
- [42] G. He, Q. Wu, Z. Li, W. Ge, D. Lv, L. Cong, "Ventilation performance of solar chimney in a test house: Field measurement and validation of plume model", *Building and Environment* **193** (2021), p. 107648.
- [43] A. T. Layeni, M. A. Waheed, B. A. Adewumi, C. N. Nwaokocho, M. Sharifpur, S. O. Tongo, R. C. Okeze, C. A. Mboreha, "Computational and sensitivity analysis of a dual purpose solar chimney for buildings", *Materials Today: Proceedings* **47** (2021), p. 4126-4136.
- [44] X.-H. Ren, L. Wang, R.-Z. Liu, L. Wang, F.-Y. Zhao, "Thermal stack airflows inside the solar chimney with discrete heat sources: Reversal flow regime defined by chimney inclination and thermal Rayleigh number", *Renewable Energy* **163** (2021), p. 342-356.
- [45] M. de Vita, F. Duronio, A. de Vita, P. de Berardinis, "Adaptive retrofit for adaptive reuse: Converting an industrial chimney into a ventilation duct to improve internal comfort in a historic environment", *Sustainability* **14** (2022), no. 6, p. 3360.
- [46] Z. Fang, W. Wang, Y. Chen, J. Song, "Structural and heat transfer model analysis of wall-mounted solar chimney inlets and outlets in single-story buildings", *Buildings* **12** (2022), no. 11, p. 1790.
- [47] J. P. Fine, S. Zhang, Y. Li, M. F. Touchie, "Analysis of solar chimney ventilation systems in high-rise residential buildings using parallel flow networks", *Building and Environment* **218** (2022), p. 109096.
- [48] P. Chung Leng, S. B. Aw, N. E. Haji Ali, G. H. T. Ling, Y. L. Lee, M. H. Ahmad, "Solar Chimneys as an Effective Ventilation Strategy in Multi-Storey Public Housing in the Post-COVID-19 Era", *Buildings* **12** (2022), no. 6, p. 820.
- [49] H. Cui, M. Han, J. Zhang, Z. Han, F. Xu, Q. Liu, "Theoretical analysis and numerical study of natural convection inside combined solar chimney", *Energy Science & Engineering* **12** (2024), no. 5, p. 2052-2071.
- [50] B. Ouedraogo, A. Ouedraogo, A. Kabore, K. Palm, D. J. Bahiebo, "Performance Evaluation of Solar Chimney Draft: Application to Ventilation", *Smart Grid and Renewable Energy* **15** (2024), no. 4, p. 107-122.

This preprint was submitted under the following conditions:

- The authors declare that the necessary Terms of Free and Informed Consent of participants or patients in the research were obtained and are described in the manuscript, when applicable.
- The authors declare that the preparation of the manuscript followed the ethical norms of scientific communication.
- The authors declare that they are aware that they are solely responsible for the content of the preprint and that the deposit in SciELO Preprints does not mean any commitment on the part of SciELO, except its preservation and dissemination.
- The authors declare that the data, applications, and other content underlying the manuscript are referenced.
- The deposited manuscript is in PDF format.
- The authors declare that the research that originated the manuscript followed good ethical practices and that the necessary approvals from research ethics committees, when applicable, are described in the manuscript.
- The authors declare that once a manuscript is posted on the SciELO Preprints server, it can only be taken down on request to the SciELO Preprints server Editorial Secretariat, who will post a retraction notice in its place.
- The authors agree that the approved manuscript will be made available under a [Creative Commons CC-BY](#) license.
- The submitting author declares that the contributions of all authors and conflict of interest statement are included explicitly and in specific sections of the manuscript.
- The authors declare that the manuscript was not deposited and/or previously made available on another preprint server or published by a journal.
- If the manuscript is being reviewed or being prepared for publishing but not yet published by a journal, the authors declare that they have received authorization from the journal to make this deposit.
- The submitting author declares that all authors of the manuscript agree with the submission to SciELO Preprints.